Journal of Analytical and Applied Pyrolysis 190 (2025) 107162

Contents lists available at ScienceDirect

Journal of Analytical and Applied Pyrolysis

journal homepage: www.elsevier.com/locate/jaap

Synergistic effect of Pd and Mo catalysts on the biomass hydropyrolysis vapor upgrading for aromatic hydrocarbons

Wanchen Zhu, Zhongyang Luo *, Feiting Miao, Longyi Liu

State Key Laboratory of Clean Energy Utilization, Zhejiang University, Hangzhou 310027, PR China

ARTICLE INFO

Keywords:
Biomass
Hydrodeoxygenation
Continuous-flow bed reactor
Pd/HZSM-5
Density functional theory

ABSTRACT

Biomass hydropyrolysis vapor upgrading (HPVU) is a promising approach for biofuel production, where metallic catalysts play a key role in oxygen removal and aromatic hydrocarbon formation. In this study, Pd/HZSM-5 and Mo/γAl_2O_3 catalysts were prepared and utilized individually or in combination to investigate their effects on poplar HPVU in a continuous-flow reactor. Meanwhile, the influence of upgrading temperature on hydrodeoxygenation (HDO) reactions was studied. At an upgrading temperature of 400 ℃, combination of Pd/HZSM-5 and Mo/γAl_2O_3 resulted in an organic phase yield of 9.19 wt%. The mass yield and selectivity of aromatic hydrocarbons reached 8.13 wt% and 93.4 %, respectively, with selectivity of C8 + monocyclic aromatic hydrocarbons accounting for 56.7 %. The overall mass balance was 96.2 %. The presence of Pd promotes hydrogenation and hydroalkylation reactions, while Mo/γAl_2O_3 enhances deoxygenation. Additionally, its mesoporous structure facilitates reactant diffusion. The density functional theory calculations confirmed that Pd could efficiently activate H_2 and thus provide hydrogen radicals for HDO on Mo/γAl_2O_3 surface, which revealed the synergistic effect of these two catalysts. This study highlights that noble-metal catalyst aided by oxophilic metal catalyst can make a significant contribution to biomass HPVU.

1. Introduction

Global energy consumption is increasing year by year. The development and utilization of sustainable energy is particularly important. Biomass is carbon-neutral and is the only carbon-containing renewable energy resource that can be directly converted into liquid fuels [1,2]. Hydropyrolysis, which means the process of pyrolysis under hydrogen atmosphere [3], has been the spotlight in decades because of its ability to efficiently convert lignocellulosic biomass into high quality liquid fuels in one step [3,4].

Although hydropyrolysis could significantly reduce oxygen functional groups, the main liquid components are still ketones and phenols. The quality of the liquid phase needs to be further refined. Various heterogeneous catalysts are widely employed in hydrodeoxygenation (HDO). Common carriers include zeolites (ZSM-5, HY, MCM-41, etc) and metal oxides (Al_2O_3, TiO_2, ZrO_2, etc) [5–8]. The abundant acidic sites and suitable pore size structure of HZSM-5 can promote cracking and aromatization reactions [8], but is prone to deactivate and produce excessive gas because of micro pore size and strong acidity. Compared to zeolite, metal oxides such as Al_2O_3 owns milder acidity [9]. Metals loaded on carriers are usually divided into hydrogenation metals (such as Pd, Ni and Co) and oxophilic metals (such as Mo and Re) [9–11]. Hydrogenation metals can promote hydrogen dissociation and ring saturation, while oxophilic metals are often used as promoters for removal of oxygen-containing functional groups.

Noble metals are well-known for hydrogen spillover effect and extremely low loading requirements [12,13]; Moreover, they could promote the reduction of auxiliary oxophilic metals to induce oxygen vacancies for oxygenates adsorption and C–O bond breaking [10,13]. While noble metals are commonly studied in hydrothermal systems, their application in pyrolysis systems has received less attention [14,15]. However, the hydropyrolysis process enables a continuous one-step conversion of biomass to liquid-phase oil, making it more suitable for industrial applications. Therefore, investigating the role of noble metals in regulating HDO products in pyrolysis systems is of significant practical importance. Similar to hydrothermal liquefaction, the upgrading temperatures in pyrolysis systems significantly influence catalytic activity and product selectivity [16,17]. Current research on biomass

Abbreviations: Ali, Aliphatic hydrocarbons; DFT, Density functional theory; HDO, Hydrodeoxygenation; HPVU, Hydropyrolysis vapor upgrading; MAHs, Monocyclic aromatic hydrocarbons; Oxy, Oxygenates; PAHs, Polycyclic aromatic hydrocarbons; Pd/Z, Pd/HZSM-5.

* Corresponding author.
E-mail address: zyluo@zju.edu.cn (Z. Luo).

https://doi.org/10.1016/j.jaap.2025.107162
Received 3 November 2024; Received in revised form 3 May 2025; Accepted 5 May 2025
Available online 6 May 2025

hydropyrolysis vapor upgrading (HPVU) primarily focuses on experimental studies, with limited exploration of theoretical investigations at the molecular level, such as density functional theory (DFT) calculations, which could provide deeper insights into catalytic and HDO reaction mechanisms [18–20].

There tends to be a strong interaction between HZSM-5 and the loaded metal, and the metal is less likely to accumulate or be lost during the reaction process, in addition, the Al_2O_3 possesses more mesopores, in this study, Pd and Mo were loaded on the surface of HZSM-5 and Al_2O_3, respectively. Therefore, this study aims to investigate the hydrogenation and hydrocracking effects of Pd/HZSM-5 assisted with the deoxygenation effect of Mo/γAl_2O_3 for biomass HPVU to obtain oil-phase products in which hydrocarbons are the main components. Pd/HZSM-5 or physically mixing it with Mo/γAl_2O_3 was selected for the refinement, and the refinement temperature was also investigated. To clarify the reaction mechanism of the noble metal Pd and the zeolite HZSM-5, the adsorption and dissociation of hydrogen on the surfaces of the two catalysts were calculated by DFT.

2. Materials and methods

2.1. Raw materials

The feedstock of poplar wood used in this study grew in the south of China. The received poplar was milled and sieved to a suitable size of 80–100 mesh and dried overnight at 105 °C before utilization. Table 1 presents the proximate and ultimate analyses of the poplar wood. Support of zeolite HZSM-5 (Si/Al molar ratio: 15) was purchased from Nankai Catalyst Factory and aluminium oxide (γAl_2O_3) was purchased from Liaoning Haitai Sci-Tech Development Co. Palladium (II) nitrate hydrate ($Pd(NO_3)_2{\cdot}2H_2O$, AR, Pd≥ 39 %, Aladdin) and Ammonium molybdate tetrahydrate ($(NH_4)_6Mo_7O_{24}{\cdot}4H_2O$, AR, 99 %, Macklin) were used to modify the HZSM-5 and γAl_2O_3, separately.

2.2. Catalysts preparation and characterizations

Since a low loading of noble metals such as Pd can achieve high dispersion and atomic utilization, while a relatively high loading of Mo can enhance HDO activity [21–24], we selected 1 wt% Pd and 15 wt% Mo to balance catalytic performance and comparability with existing studies. Catalysts were prepared with a wet impregnation method. The detailed information is shown in Supporting Information. Prior to the experiment, the catalyst was reduced in H_2 flow (80 ml min^{-1}) at 500 °C for 5 h and then passivated in N_2 flow containing 5 % O_2 at room temperature for 30 min. Mo/γAl_2O_3 was prepared by the same method but without passivation. To determine the properties of catalysts, analysis of N_2 adsorption–desorption, X-ray diffraction (XRD), X-ray photoelectron spectroscopy (XPS), NH_3 temperature-programmed desorption (NH_3-TPD) were carried out. The detailed method is shown in Supporting Information.

2.3. Experimental system and conditions

The experiments were conducted in a bench-scale continuous flow high-pressure fixed-bed system and the diagram of the reaction system is shown in Fig. 1, which mainly consists of two tandem reactors of pyrolysis and refining, connected in the middle by a thermostat box with a built-in char tank for insulating the pipeline. About 40 g of dried biomass feedstock (80–100 mesh) was put into the silo and continuously fed to the pyrolysis oven through the magnetic screw system at a rate close to 0.2 g/min, with the pyrolysis temperature of 500 °C. Carrier gas of H_2 was fed into the system from the silo and the top of the pyrolysis oven, with a flow rate of 1 L/min each. The char obtained from the pyrolysis of the biomass fell into the char tank, and the hydropyrolysis vapor were sent into the refining section, and 30 g catalysts were placed in the middle of the refining tube before the reaction.Since the objective of the study is to investigate the catalytic performance, the WHSV was set to 0.5 $g{\bullet}h^{-1}$. And the refining temperature is 300–400 °C. When two catalysts were used, they were physically pre-mixed before being loaded into the refining tube. The mass ratio of catalysts to reacted poplar is approximately 1:1. After the reaction, the product is sequentially passed through the water cooling system (10 °C), the two-stage dry ice-acetone condensation system (-78 °C) and a filter tank to complete the collection of liquid-phase products, and the final non-condensable gas is collected into gas bags. Table S1 lists the scenarios of catalysts utilization and conditions.

Table 1
Proximate, ultimate and HHV analysis results of poplar.

Proximate analysis (wt%)	value	Ultimate analysis (wt%)	value
Moisture	0.52	C	49.36
volatiles	83.42	H	5.67
Fixed carbon	15.61	O	43.50
Ash	0.45	N	0.10
Total	100	S	0.46
HHV (MJ/kg)	18.96	Total	99.09

The remaining poplar wood was recovered at the end of the reaction and the mass of raw material dropped by the reaction was calculated. The catalyst was collected and weighed after the reaction, and the difference in mass between before and after the reaction was the mass of carbon deposits. The liquid phase products are divided into the organic phase, which is mainly composed of hydrocarbons (C4 + aliphatic hydrocarbons, C6 + monocyclic aromatic hydrocarbons and C10 + polycyclic aromatic hydrocarbons), and the aqueous phase, which is mainly water and contains a small amount of small molecule oxygenated compounds such as acids and ketones.

The oil-phase products were analyzed by GC-MS (gas chromatography–mass spectrometry, GC7890B, MSD5977B), for component analysis, and quantitative calculations of the main hydrocarbon fractions were carried out by the external standard method. The products were divided into monocyclic aromatic hydrocarbons (MAHs), polycyclic aromatic hydrocarbons (PAHs), aliphatic hydrocarbons (Ali), phenols and other oxygenates (Oxy, i.e. acids, alcohols, aldehydes, ketones and furans). Fig. S1 presents the corresponding spectrum of the optimal liquid phase. Gas phase products were analyzed and quantified by GC-FID/TCD. The detailed collection and analyzing method of products are shown in Supporting Information.

$Yield_i$ (wt%), $selectivity_i$ (%) and carbon yield (%) of the products were calculated as follows:

$$\text{yield}_i = \frac{m_i}{m_{biomass}} \times 100\% \quad (1)$$

$$\text{selectivity}_i = \frac{\text{peak area}_i}{\text{peak area}_{total}} \times 100\% \quad (2)$$

$$\text{carbon yield of product} = \frac{\textit{the carbon mass in products}}{\textit{the total carbon mass in feedstock}} \times 100\% \quad (3)$$

Where m_i and peak area_i mean the mass yield and the peak area of a certain product, and i represents the total solid, gas, liquid products or a specific kind of hydrocarbons. $M_{biomass}$ is the mass of biomass that hydropyrolyzed and peak area_{total} is the total peak area of detected components by GC-MS.

2.4. Computational methods

All DFT calculations were conducted using the Vienna ab initio Simulation Package (VASP). The exchange-correlation energy was described using the GGA-PBE functional [25], and the projector

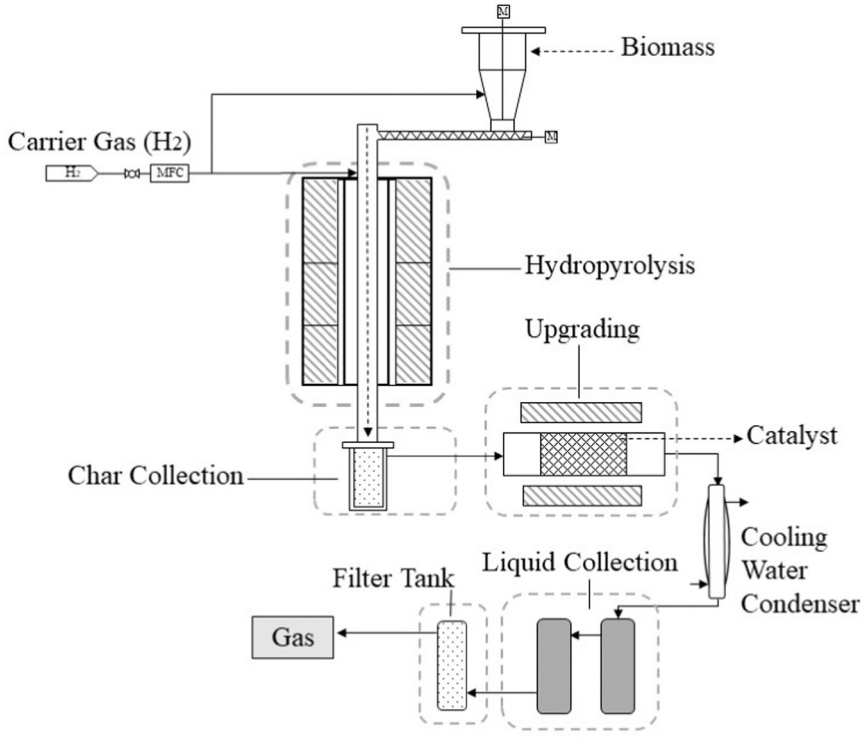

Fig. 1. The schematic diagram of continuous flow high-pressure fixed-bed system.

augmented wave (PAW) method was employed [26]. Additionally, the DFT-D3 method was used to account for van der Waals interactions within the system [27,28]. An energy cut-off of 400 eV was applied. The Pd (1 1 1) surface was modeled as four layers with the bottom two layers fixed during geometry optimization and a supercell (4 ×4) was built with a 15 Å vacuum layer. The k-points was 3 × 3×1 for the Brillouin zone. The HZSM-5 model was downloaded directly from International Zeolite Association (IZA) database and six certain Si atoms were substituted with Al atoms to achieve the Si/Al ratio of 15 [29], and the k-points was 1 × 1 × 1. The optimized geometry of HZSM-5 is in Fig. S3. Lattice parameters and ionic positions were fully relaxed, with total energy converging within 10^{-6} eV and forces being less than 0.02 eV/Å. The Cl-NEB method was utilized for transition-state search.

3. Results and discussion

3.1. Characterization of catalysts

The XRD results are shown in Fig. 2a and b, the intensity of the diffraction peaks of Pd/HZSM-5 and Mo/γAl_2O_3 decreased compared with support, which means that part of the structure turned into amorphous state. But on the whole, the crystalline structure of the carrier was not damaged by the loaded metal particles.

The forms and valence states of metal elements presented on the surface of the catalyst were analyzed using XPS. As observed in Fig. 2c, the Pd/HZSM-5 catalyst had two peaks at binding energies of 340.5 eV and 335.4 eV [17,30], corresponding to Pd $3d_{3/2}$ and Pd $3d_{5/2}$, respectively, which proved that the form of monomer Pd was the active valence state. In the XPS spectra of Mo/γAl_2O_3 catalyst shown in Fig. 2d, there were peaks at binding energies of 230.9 eV, 233.6 eV, 232.8 eV and 235.6 eV [9,16,31], and the first two and the last two correspond to Mo $3d_{3/2}$ and Mo $3d_{5/2}$, respectively, which indicated that Mo exists in the form of Mo^{5+} and Mo^{6+}. Some atoms of Mo were reduced, and this would generate oxygen vacancies which facilitated the cleavage of C-O bond [32,33].

The HZSM-5 and γAl_2O_3 differed significantly in the pore structure, as shown in Table 2, the specific surface area of the micropores (S_{micro}) of the HZSM-5 modified by Pd decreased slightly, probably due to the partial coverage of the metal particles, whereas the specific surface area of the mesopores (S_{meso}) increased by nearly 1/3. At the same time, compared with the pristine HZSM-5, the pore volume of Pd/HZSM-5 was basically unchanged. In contrast, the catalyst Mo/γAl_2O_3 owned only about half of the specific surface area of the latter compared with HZSM-5, which contained almost no micropores, while the mesoporous specific surface area was close to 21 times that of the original HZSM-5, and the pore volume of the Mo/γAl_2O_3 catalyst was much larger as well. From Fig. 2e, it could be found that positions of the pore distribution peaks of HZSM-5 catalyst were not changed after metal loading, which are located at 0.6 nm and 2.0 nm, where the pore size reached maximum. Pore size distribution of Mo/γAl_2O_3 is located about 10 nm (Fig. S4). Therefore, γAl_2O_3 could facilitate the diffusion of intermediates and HZSM-5 could improve the hydrocracking of large molecules.

The results of the acidity characterization of the catalysts are shown in Fig. 2f and Table 2. Strong acid peaks were evident between 450 and 500 °C for HZSM-5 and Pd/HZSM-5, and not obvious in the results for Mo/γAl_2O_3 [31]. All three catalysts had obvious strong diffraction peaks in the 100–150 °C temperature interval [31]. For HZSM-5, the introduction of Pd changed the original acidic structure, and the total acid amount was reduced from 5.98 mmol/g to 5.18 mmol/g, which increased the number of weak acid sites and correspondingly decreased the strong acid sites. The introduction of Pd optimize the acid site distribution of the support. Compared to HZSM-5, Mo/γAl_2O_3 owned milder acidity.

3.2. Effect of Pd for HDO and Mo in auxiliary

To determine the role of the synergistic HDO effect of Pd/HZSM-5 and Mo/γAl_2O_3, we evaluated the performance of Pd/HZSM-5 alone and in combination with Mo/γAl_2O_3 in the HPVU, and the results of the product analysis are shown in Fig. 3. The liquid and non-condensable gas phase mass yields differed significantly between the two cases (Fig. 3a), in which the total liquid and oil phase yields were only 37.2 wt

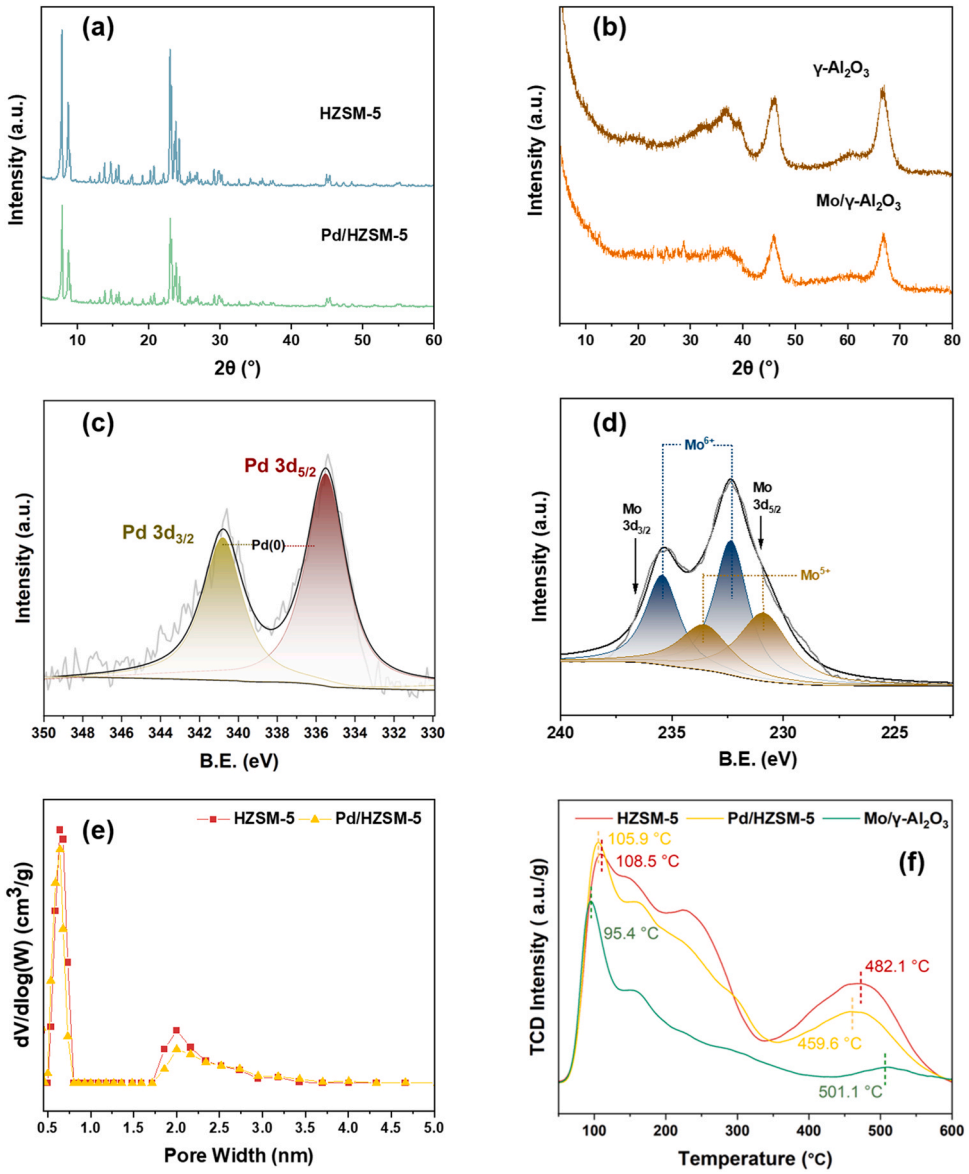

Fig. 2. XRD profiles of (a) the parent HZSM-5 and Pd modified Pd/HZSM-5, (b) support γAl_2O_3 and Mo modified Mo/γAl_2O_3, XPS spectra of (c) Pd in Pd/HZSM-5 and (d) Mo in Mo/γAl_2O_3, (e) the pore size distribution of HZSM-5 and Pd/HZSM-5, (f)NH_3-TPD analysis profile of HZSM-5, Pd/HZSM-5 and Mo/γAl_2O_3.

Table 2
The porosity characteristics of catalysts.

Catalyst	S_{bet}	S_{micro}	S_{meso}	V_{total}	V_{micro}	V_{meso}	Total acid	Content (%)	
	m^2/g	m^2/g	m^2/g	cm^3/g	cm^3/g	cm^3/g	mmol/g	Weak	Strong
HZSM−5	424	414	9.49	0.19	0.17	0.02	5.98	71.9	28.1
Pd/Z	397	385	12.4	0.18	0.16	0.02	5.18	77.1	22.9
Mo/γ-Al_2O_3	229	13.0	216	0.54	0.01	0.53	2.27	88.2	11.8

% and 2.79 wt% for Pd/Z alone and increased to 46.8 wt% and 9.19 wt % with hydrocarbon mass yields of 2.02 wt% and 8.13 wt%, respectively (Fig. 3b). Accordingly, the yield of former non-condensable gases was as high as 37.5 wt%, while that of the latter was only 28.1 wt%. The overall mass balance reached 96.2 %. From the characterization results, it could be seen that the main active site of the HZSM-5 was Brønsted acid site, which was capable of promoting C-O and C-C scission, and the hydrocracking reaction was enhanced under relatively high temperature and high pressure operating conditions [34].

The oil phases obtained from both catalytic scenarios were mainly composed of aromatic hydrocarbons and with low oxygen content, the selectivity of aromatic hydrocarbons was 93.4 % and 88.7 % when the catalysts were Pd/HZSM-5 and the mixture, respectively. The selectivity of the C8 + MAHs was 56.7 % of the mixture. The oxygen-containing compounds in the final oil phase were mainly phenolics, which were 3.72 % and 6.21 %, respectively. However, due to the overpowering of HZSM-5 cleavage, with action of the Pd/HZSM-5 alone, alkane products were not detected, and after mixing the two catalysts, the cracking effect was moderated and Pd promoted the generation of small molecule alkanes such as pentane (Fig. 3c) [23].

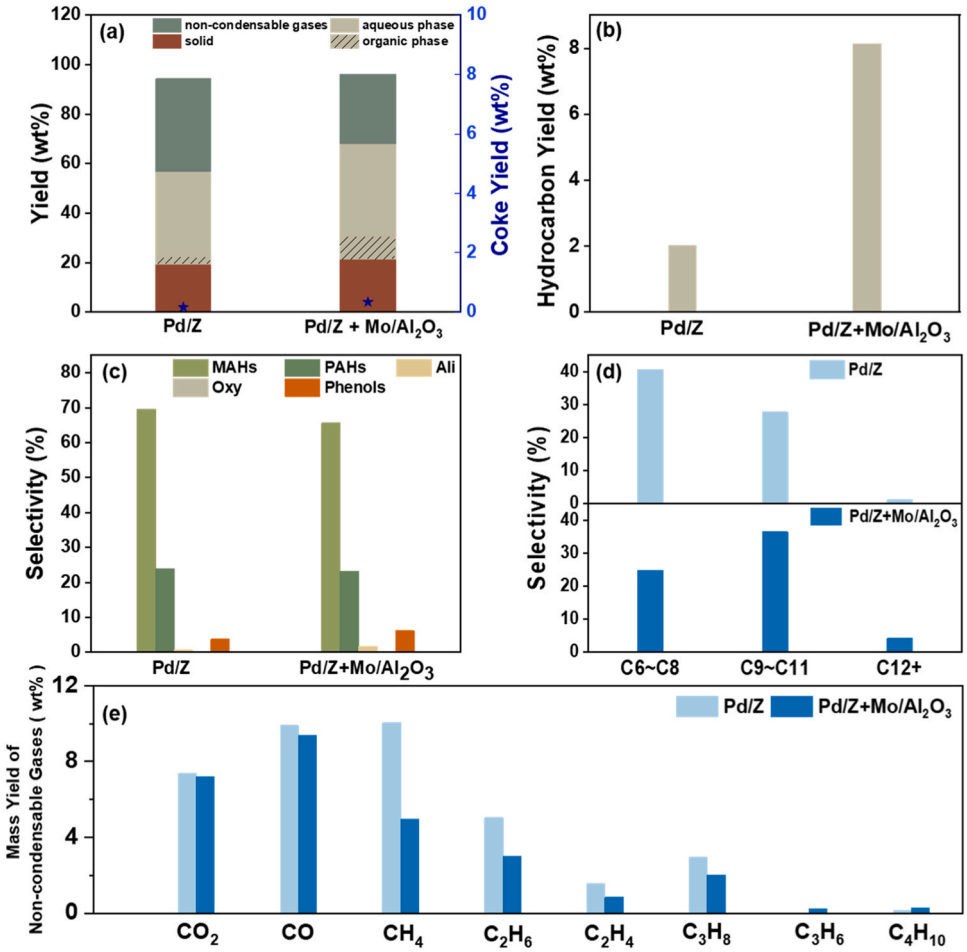

Fig. 3. Products of upgrading over Pd/HZSM-5 and Pd/HZSM-5 physically mixed with Mo/Al_2O_3. (a) Mass yield of each phase and total mass balance; (b) Mass yield of hydrocarbons in liquid; (c) Selectivity of main liquid components; (d) Carbon number distribution of hydrocarbons in liquid; (e) Mass yield of main gas components. (Hydropyrolysis temperature 500 °C, upgrading temperature 400 °C, pressure 1 MPa, catalyst 30 g).

Fig. 3d presented the carbon number distribution of the MAHs, in which Pd/HZSM-5 upgrading produced more MAHs with C6~C8 (e.g., benzene, toluene, ethylbenzene, and xylenol, namely, BTEX), and the selectivity of the MAHs with higher carbon numbers decreased significantly, After the introduction of the mild acidic oxophilic catalyst of Mo/γAl_2O_3, the selectivity of MAHs in C6~C8 decreased from 40.7 % to 24.9 %, while that in C9~C11 increased from 27.8 % to 36.5 %. After mixing the two catalysts, the selectivity of MAHs was close to that of Pd/HZSM-5 alone while the yield of the oil phase was significantly increased, and the selectivity of aromatics was higher in the case of the higher carbon number, which indicated that there was a favorable synergistic interaction between the two catalysts of different functionalities [7,35]. According to Fig. 3e, decarbonylation and decarboxylation are still the more dominant deoxygenation reactions. In addition, the yield of small molecule gaseous alkanes reached 20.8 wt% in the absence of Mo/γAl_2O_3, mainly from deoxygenated cleavage of cellulose and hemicellulose pyrolysis derivatives such as furfural, as well as phenolic branched chain C-C and C-O breakage, indicating that Pd/HZSM-5 catalysis alone caused relatively more carbon loss [36].

3.3. Effect of catalytic upgrading temperature

The above results demonstrated that Pd/HZSM-5 dominated the formation of aromatic hydrocarbons while Mo/γAl_2O_3 assisted in modification of the products distribution. To further verify their synergistic effect during HDO, the upgrading temperature was investigated at 300 °C, 350 °C and 400 °C [9,37,38]. The distribution of the three-phase products is shown in Fig. 4a, and the liquid phase yields were as follows, from highest to lowest: 48.2 wt% (300 °C) > 48.1 wt% (350 °C) > 46.8 wt% (400 °C), which indicated that higher temperatures promoted the cracking reaction. However, the oil phase yield dropped to about 7.00 wt% while the temperature dropped, and the mass balance of the system was around 96.0 wt%. The yield of hydrocarbons also decreased from 7.59 wt% to about 6.00 wt% (Fig. 4b), however, yield of non-condensable gases obtained for the condition with the lower refining temperature was also lower than 400 °C, and the coke yield increased significantly to about 5.00 wt%, while the weight of the catalyst before and after the reaction at 400 °C remained almost unchanged. The temperature decreased, on the one hand, the cracking reaction of HZSM-5 and the deoxygenation reaction of Mo/γAl_2O_3 were inhibited, and small molecule hydrocarbons were cyclized to MAHs, and on the other hand, the hydrogen radicals provided by the dissociated hydrogen from Pd decreased, thus more MAHs were further aromatized to coke precursors such as PAHs, which led to an increase in the carbonaceous deposits [17,39].

From the distribution of liquid phase components (Fig. 4c), the selectivity of PAHs increased significantly with decreasing temperature, which partly confirmed the reason for the increase of coke as mentioned above, and the accelerated deactivation of the catalyst resulted in higher oxygen content of the liquid phase, with the selectivity of oxygenated compounds as phenols and ketones exceeded 20.0 % at 300 °C, which demonstrated that the upgrading temperature had a significant effect on the HDO of the catalysts [40,41], and the selectivities of MAHs were as follows: 65.6 % (400 °C) > 49.6 % (350 °C) > 43.2 % (300 °C). As

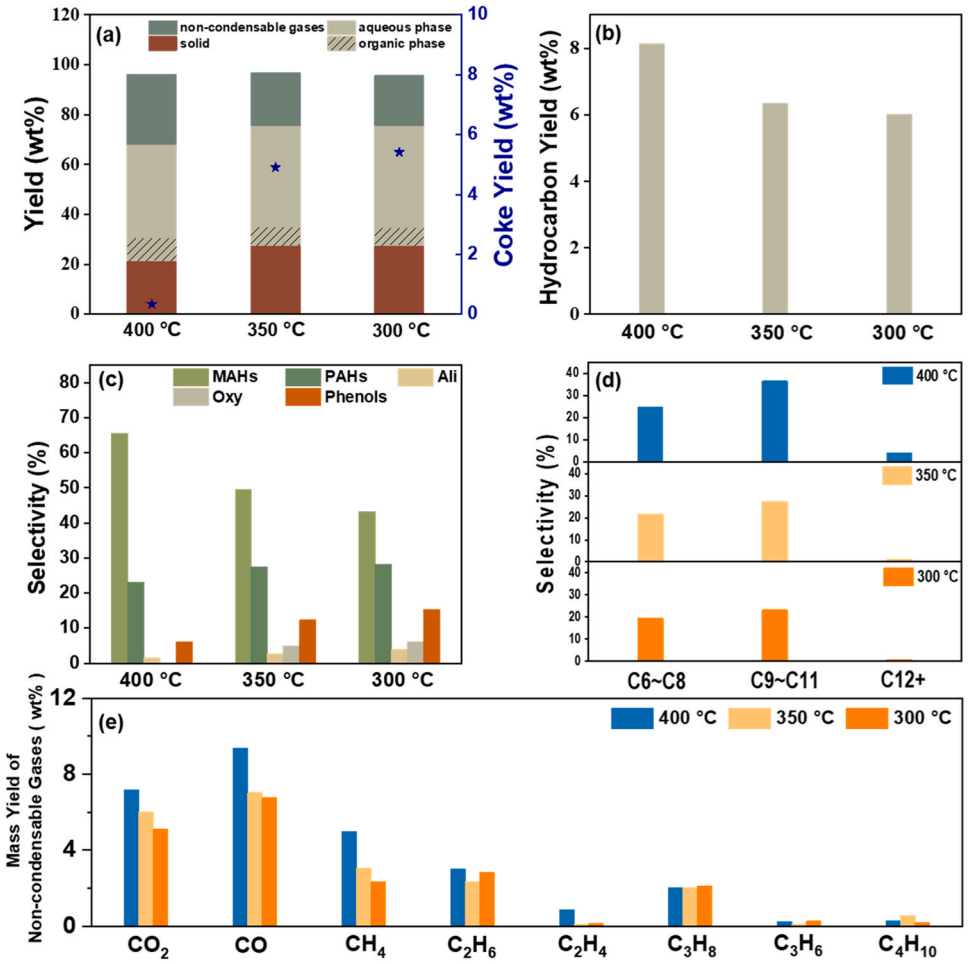

Fig. 4. Products of upgrading over different upgrading temperature. (a) Mass yield of each phase and total mass balance; (b) Mass yield of hydrocarbons in liquid; (c) Selectivity of main liquid components; (d) Carbon number distribution of hydrocarbons in liquid; (e) Mass yield of main gas components. (Hydropyrolysis temperature 500 °C, pressure 1 MPa, catalyst 30 g).

shown in Fig. 4d, the selectivity of MAHs in each carbon number distribution region also decreased with the decrease of temperature, and the selectivity of MAHs in C9~C11 decreased most obviously from 36.5 % to 27.1 % at 350 °C and 23.2 % at 300 °C, respectively, while the selectivity of alkanes increased from 1.62 % to 3.98 %, which showed that the hydrogenation reaction was promoted by the catalysts at the relatively low refining temperature, while the HDO and aromatization reaction activities were more active at 400 °C [9,16]. This was corroborated by the component distributions of non-condensable gases, which showed that the selectivity of CO and CO_2 at 400 °C was significantly higher than that at 350 °C and 300 °C as seen in Fig. 4e, and CH_4 had the highest selectivity at 400 °C due to promoted cracking effects under high temperature.

Although at relatively low temperatures the hydrogenation activity of noble metals was enhanced and the saturation reaction was more preferred, the increase in oxygenate compounds selectivity was more detrimental to the quality of the bio-oil. A comprehensive consideration of oil phase yield, hydrocarbon selectivity, and oxygen content suggested that 400 °C was a relatively favorable temperature for upgrading. And the overall carbon balance achieved 95.6 wt% when the upgrading temperature was 400 °C. The carbon yield of the individual product phases are shown in Table 3. The picture of liquid product is shown in Fig. S2.

Table 3
Carbon yield of part of the products.

Yield	Carbon yield (wt%)
Organic phase	18.1
Non-condensable gas	42.9
Char	34.6
Total	95.6

3.4. *Effect of the metal site and zeolite acid site*

With the upgrading temperature fixed, to determine the promotion effect of noble metals and HZSM-5 on the HDO reaction, in this study, Pd/HZSM-5, HZSM-5 were physically mixed with Mo/γAl_2O_3 for HDO respectively and compared with Mo/γAl_2O_3 alone, and the results are shown in Fig. 5. Fig. 5a indicated that Mo/γAl_2O_3 mainly catalyzed the deoxygenation reaction, and the hydrogen radicals in the reaction basically came from the dissociation of hydrogen molecules, and basically did not contain active sites with strong acidity, and the hydrocracking reaction was not prominent, therefore, the yields of the liquid phase (49.3 wt%) and the oil phase (10.3 wt%) were relatively high, while the large mesoporous area of γAl_2O_3 also provided adhesion space for the generation of coke (4.19 wt%). After the introduction of HZSM-5, the oxygenated compounds such as phenols and ketones underwent direct and indirect deoxygenation reactions such as hydrogenolysis, and the yield of non-condensable gases was increased from 23.1 wt% to

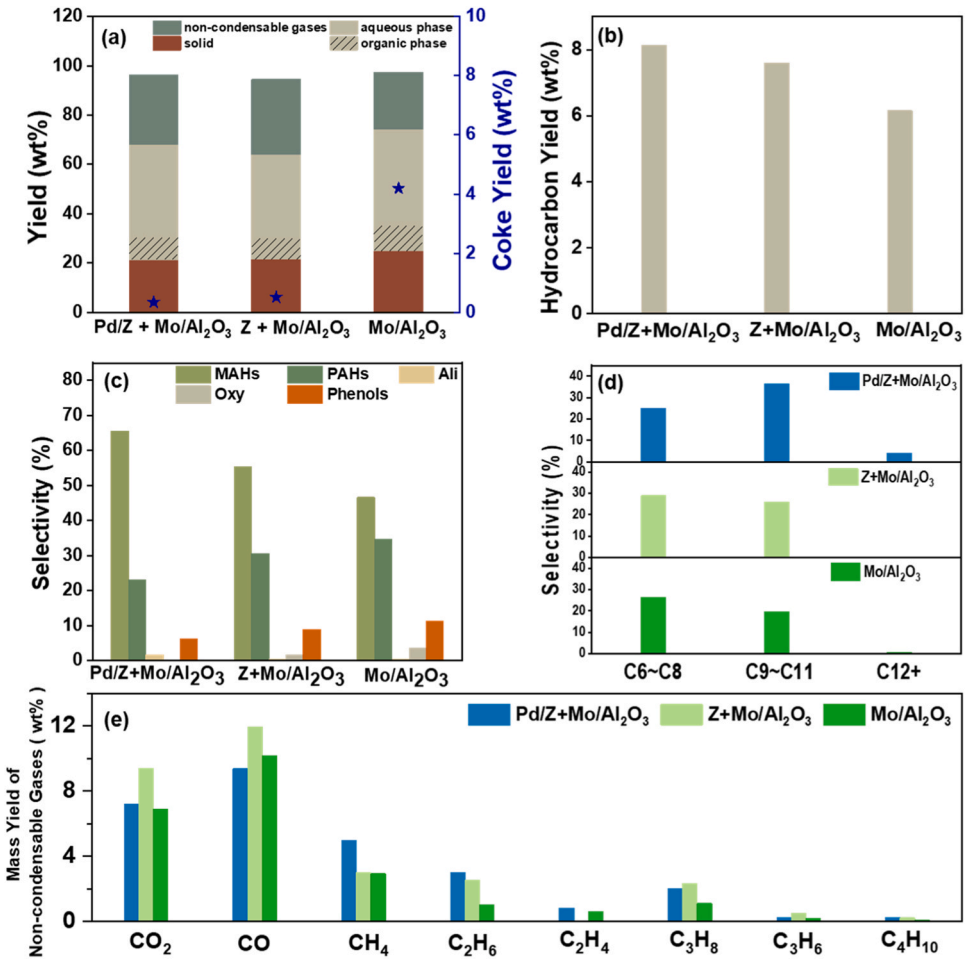

Fig. 5. Products of upgrading over different catalysts. (a) Mass yield of each phase and total mass balance; (b) Mass yield of hydrocarbons in liquid; (c) Selectivity of main liquid components; (d) Carbon number distribution of hydrocarbons in liquid; (e) Mass yield of main gas components. (Hydropyrolysis temperature 500 °C, upgrading temperature 400 °C, pressure 1 MPa, catalyst 30 g).

30.5 wt%, while the liquid-phase and oil-phase yields were reduced to 42.4 wt% and 8.62 wt%, respectively. Based on this, the liquid and oil phase yields of HZSM-5 loaded with Pd were further increased to 46.8 wt% and 9.19 wt%, while the yield of non-condensable gases was only 28.1 wt%. It could also be seen from Fig. 5b that the hydrocarbon yields were reduced to 7.59 wt% and 6.15 wt% with and without HZSM-5, respectively, compared with the presence of Pd metal sites. Combined with the acidity characterization results, it could be seen that the introduction of Pd changed the acidity of the catalyst, reducing the strong acid sites, and was able to generate relatively more liquid phase [42,43]. The combination of Pd/HZSM-5 and Mo/γAl_2O_3 exhibited improved upgrading performance for production of aromatic hydrocarbons, as shown in the comparison with previous studies in Table S2.

Fig. 5c presents the distribution of liquid phase components in detail, the HZSM-5 contained more Brønsted acid site, which promoted the aromatization reaction, and compared with only Mo/γAl_2O_3, the aromatics selectivity was increased from 81.1 % to 85.9 %. After the introduction of Pd, the number of acidic sites increased and the dissociation of hydrogen was promoted, which effectively reduced the over-coupling of MAHs to generate coke precursors such as PAHs, and the aromatic hydrocarbons were further increased to 88.7 %, of which the selectivity of MAHs reached 65.6 %. Oxygenated compounds were also found to reach the relatively lowest level of selectivity (6.32 %). The carbon number distributions of the MAHs obtained from the three scenarios were also significantly different, as shown in Fig. 5d, the HZSM-5 improved the selectivity of MAHs with C6∼C11, and due to the stronger cleavage ability, more MAHs with carbon numbers greater than 11 were not detected. In addition, under the effect of Pd, some small oxygenated molecules, such as alcohols and aldehydes, would be added to the carbon ring or branched chain of the aromatic hydrocarbon by hydroalkylation and aldol condensation reactions [44,45]. The relatively low yields of CO and CO_2 in the presence of Pd suggested that the noble metal further promoted deoxygenation by dehydration to retain more carbon content in the final liquid phase, and the highest yields of the two kinds of gas were obtained when the HZSM-5 and γAl_2O_3 were physically mixed, which suggests that the HZSM-5 mainly facilitated decarboxylation and decarbonylation reactions (Fig. 5e).

3.5. Catalytic mechanism by DFT computation

Experimental results showed that Pd was superior to HZSM-5 in HDO reaction activity. To clarify the promotion mechanism of noble metals Pd and HZSM-5 theoretically, DFT calculations of the adsorption energy and dissociation ease of hydrogen on the Pd (111) surface and inside HZSM-5 were carried out in this study. As shown in Fig. 6c, the analysis of the TEM results of Pd/HZSM-5 led to the corresponding Pd (111) surface (PDF#87–0637). Therefore, the adsorption energies of hydrogen at different adsorption positions on the Pd (111) surface were calculated, as shown in Fig. 6a, and a relatively stable adsorption configuration of hydrogen was finally obtained at the FCC position, which was in agreement with the calculation results of the previous related studies [46,47]. The adsorption energy was −0.46 eV, indicating that Pd could easily capture and immobilize hydrogen from the gas phase, effectively improving the efficiency of hydrogen utilization. Compared with Pd, the

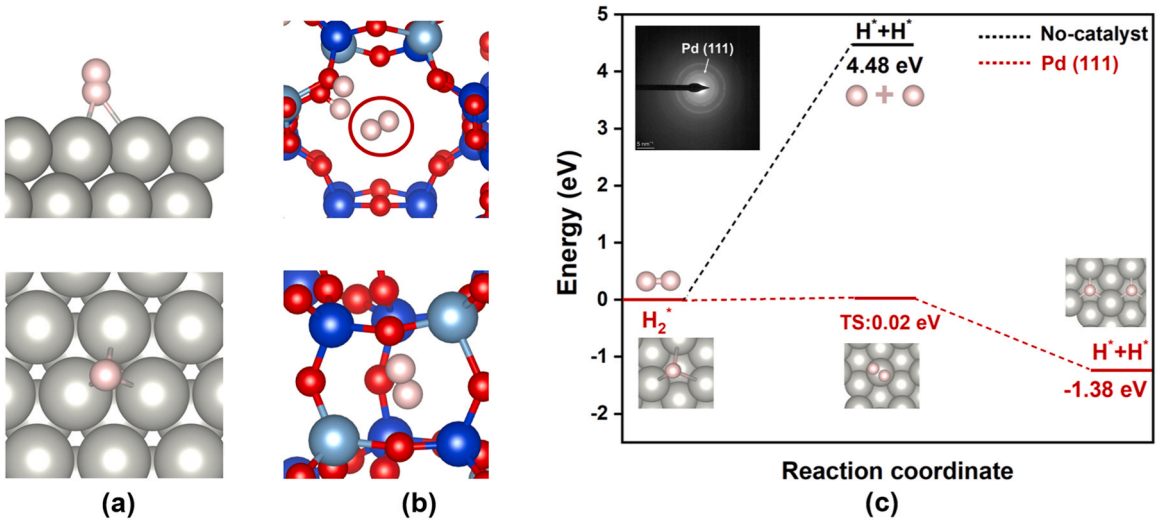

Fig. 6. Adsorption energy of H_2 (a) on Pd (111), and (b) HZSM-5, both with front and top view; (c) Potential energy profile for H_2 dissociation on Pd (111) and TEM image of Pd/HZSM-5. The grey, pink, bule, cyan, and red present the Pd, H, Si, Al and O, respectively. The red circle in (b) shows the adsorbed hydrogen while other hydrogen atoms in (b) are used to balance the charge.

adsorption energy of hydrogen inside HZSM-5 was low, and the screening calculation of different acidic sites of HZSM-5 (Fig. S5 and Table S3) resulted in an adsorption energy of −0.27 eV in the relatively steady state (Fig. 6b). On the one hand, hydrogen that is too small compared to the zeolite pore size were more inclined to remain in a molecular state and leave the zeolite molecules through the micropores, and on the other hand, it was difficult for zeolites to provide many electrons for adsorption of hydrogen as metals do.

Calculations of the dissociation energy of hydrogen in the gas phase were carried out and it was learned that the energy barrier for the decomposition of hydrogen into atoms in the absence of a catalyst was high, reaching 4.48 eV. As illustrated in Fig. 6c, by calculating the processes of hydrogen dissociation on the surface of Pd (111), it could be seen that the dissociation of hydrogen into atoms under the effect of the Pd only needed to overcome an energy barrier of 0.02 eV, which was significantly lower than that in the gas-phase environment, and the adsorption energies of the dissociated two hydrogen atoms on the surface of Pd (111) reached −1.38 eV. However, according to the calculation results, it could be concluded that it was difficult for the dissociation reaction of hydrogen to occur on the zeolite surface.

According to the calculations, the hydrogen radicals for the HDO reaction in the absence of Pd basically originated from the gas phase, and Pd greatly promoted the dissociation of hydrogen to provide a large number of hydrogen radicals for the subsequent deoxygenation and hydrogenation reactions, and these were in line with experimental results, that introduction of Pd enhanced the HDO reaction and thus effectively increasing the selectivity of the target products and reducing the oxygen content compared to HZSM-5 alone.

4. Conclusions

In this study, the combination of hydrogenation catalyst Pd/HZSM-5 and deoxygenation catalyst Mo/γAl_2O_3 were employed in the HPVU of poplar to produce bio-oil mainly consists of aromatic hydrocarbons. The main conclusions are as follows:

The Pd/HZSM-5 catalyzed the aromatization and hydrogenation reactions with remarkable effects, and the synergistic effect aided by Mo/γAl_2O_3 can improve the oil phase yield to 9.19 wt% with the total mass balance reaching 96.2 %, while maintaining the high selectivity of MAHs as 65.6 % (C8 + was 56.7 %). The refining temperature had a significant effect on the catalytic activity. The catalysts consisted of Pd/HZSM-5 and Mo/γAl_2O_3 obtained the highest hydrocarbon selectivity (93.4 %) and the lowest oxygenate selectivity (3.95 %) at 400 °C, while 300 and 350 °C promoted alkane selectivity, which suggested that relatively mild refinement temperature can promote saturation and increase carbon yield.

Introducing Pd into HZSM-5 optimized the acidity, and the organic phase yield was improved compared with the HZSM-5, in which the hydrocarbon mass yield reached 8.13 wt% and the selectivity of MAHs (>C9) reached 40.7 %. Combined with DFT calculations, it was found that Pd could adsorb hydrogen more easily than HZSM-5 and could greatly reduce the hydrogen dissociation energy barrier, providing sufficient hydrogen radicals for the HDO reaction to inhibit the overcoupling reaction.

A preliminary attempt to employ noble metal catalyst for hydrogenation and hydroalkylation reactions during HPVU of biomass was conducted, which aided by non-noble metal catalyst for deoxygenation. This study aims to provide implications for the potential application of noble metal-based catalysts in hydropyrolysis system.

CRediT authorship contribution statement

Zhu Wanchen: Writing – original draft, Investigation, Formal analysis, Conceptualization. **Luo Zhongyang:** Supervision, Project administration, Funding acquisition. **Miao Feiting:** Investigation, Formal analysis. **Liu Longyi:** Investigation.

Declaration of Competing Interest

The authors declare that they have no known competing financial interests or personal relationships that could have appeared to influence the work reported in this paper.

Acknowledgement

This work was supported by the National Natural Science Foundation of China, No. 52236011.

Appendix A. Supporting information

Supplementary data associated with this article can be found in the online version at doi:10.1016/j.jaap.2025.107162.

Data availability

No data was used for the research described in the article.

References

[1] R. Batten, M. Karanjikar, S. Spatari, A sustainable aviation fuel pathway from biomass: life cycle environmental and cost evaluation for dimethylcyclooctane jet fuel, Sustain. Energy Fuels 8 (9) (2024) 1924–1935, https://doi.org/10.1039/D3SE01470C.

[2] J.C. Serrano-Ruiz, J.A. Dumesic, Catalytic routes for the conversion of biomass into liquid hydrocarbon transportation fuels, Energy Environ. Sci. 4 (1) (2011) 83–99, https://doi.org/10.1039/C0EE00436G.

[3] T.M.H. Dabros, M.Z. Stummann, M. Høj, P.A. Jensen, J.-D. Grunwaldt, J. Gabrielsen, P.M. Mortensen, A.D. Jensen, Transportation fuels from biomass fast pyrolysis, catalytic hydrodeoxygenation, and catalytic fast hydropyrolysis, Prog. Energy Combust. Sci. 68 (2018) 268–309, https://doi.org/10.1016/j.pecs.2018.05.002.

[4] N.Z. Uludere Aragon, N.C. Parker, A. VanLoocke, J. Bagley, M. Wang, M. Georgescu, Sustainable land use and viability of biojet fuels, Nat. Sustain. 6 (2) (2022) 158–168, https://doi.org/10.1038/s41893-022-00990-w.

[5] J. Su, K. Miao, Y. Zhao, T. Li, Z. Zhao, G. Luo, K. Wang, Production of gasoline components from biomass catalytic hydropyrolysis using zeolite-based bifunctional catalysts, Biomass Convers. Biorefin. 14 (9) (2024) 10347–10359, https://doi.org/10.1007/s13399-022-02995-z.

[6] P. Yan, I. Nur Azreena, H. Peng, H. Rabiee, M. Ahmed, Y. Weng, Z. Zhu, E. M. Kennedy, M. Stockenhuber, Catalytic hydropyrolysis of biomass using natural zeolite-based catalysts, Chem. Eng. J. 476 (2023) 146630, https://doi.org/10.1016/j.cej.2023.146630.

[7] Y. Xu, G. Nie, X. Jiang, H. Wang, G. Yang, Z. Yan, J.-J. Zou, H. Yu, S. Yu, Y. Liu, Synthesis of 1-hexanol by highly selective hydrodeoxygenation of 5-Hydroxymethylfurfural using Ni/MCM-41 and Pt-WOX/t-ZrO2, Chem. Eng. J. 487 (2024) 150695, https://doi.org/10.1016/j.cej.2024.150695.

[8] Y. Zhang, J. Wang, J. Jiang, X. Guo, Enhancing coking resistance of ZSM-5 in the conversion of pine sawdust into oxygen-free bio-aromatic hydrocarbons through tandem catalytic hydropyrolysis/vapor-phase hydrotreatment, Energy 289 (2024) 130001, https://doi.org/10.1016/j.energy.2023.130001.

[9] F. Miao, Z. Luo, Q. Zhou, L. Du, W. Zhu, K. Wang, J. Zhou, Study on the reaction mechanism of C8+ aliphatic hydrocarbons obtained directly from biomass by hydropyrolysis vapor upgrading, Chem. Eng. J. 464 (2023) 142639, https://doi.org/10.1016/j.cej.2023.142639.

[10] M. Liu, J. Zhang, L. Zheng, G. Fan, L. Yang, F. Li, Significant promotion of surface oxygen vacancies on bimetallic CoNi Nanocatalysts for Hydrodeoxygenation of Biomass-Derived Vanillin to Produce Methylcyclohexanol, ACS Sustain. Chem. Eng. 8 (15) (2020) 6075–6089, https://doi.org/10.1021/acssuschemeng.0c01015.

[11] M.M. Ambursa, J.C. Juan, Y. Yahaya, Y.H. Taufiq-Yap, Y.-C. Lin, H.V. Lee, A review on catalytic hydrodeoxygenation of lignin to transportation fuels by using nickel-based catalysts, Renew. Sustain. Energy Rev. 138 (2021) 110667, https://doi.org/10.1016/j.rser.2020.110667.

[12] Y. Geng, H. Li, Hydrogen spillover-enhanced heterogeneously catalyzed hydrodeoxygenation for biomass upgrading, ChemSusChem 15 (8) (2022) e202102495, https://doi.org/10.1002/cssc.202102495.

[13] S. Fan, M. Zhang, H. Li, Zirconium-doped enhanced the biomass hydrodeoxygenation over extremely low-loaded Pd catalysts, Fuel 315 (2022) 123060, https://doi.org/10.1016/j.fuel.2021.123060.

[14] G.B. Strapasson, L.S. Sousa, G.B. Báfero, D.S. Leite, B.D. Moreno, C.B. Rodella, D. Zanchet, Acidity modulation of Pt-supported catalyst enhances C-O bond cleavage over acetone hydrodeoxygenation, Appl. Catal. B Environ. 335 (2023) 122863, https://doi.org/10.1016/j.apcatb.2023.122863.

[15] Y. Tian, L. Guo, C. Qiao, Z. Sun, Y. Yamauchi, S. Liu, Dynamics-driven tailoring of sub-nanometric Pt-Ni bimetals confined in hierarchical zeolite for catalytic hydrodeoxygenation, Appl. Catal. B Environ. 336 (2023) 122945, https://doi.org/10.1016/j.apcatb.2023.122945.

[16] T. Li, J. Su, H. Wang, C. Wang, W. Xie, K. Wang, Catalytic hydropyrolysis of lignin using NiMo-doped catalysts: catalyst evaluation and mechanism analysis, Appl. Energy 316 (2022) 119115, https://doi.org/10.1016/j.apenergy.2022.119115.

[17] J. Wang, J. Jiang, D. Li, X. Meng, A.J. Ragauskas, Integrated hydropyrolysis and vapor-phase hydrodeoxygenation process with Pd/Al2O3 for production of advanced oxygen-containing biofuels from cellulosic wastes, Fuel Process. Technol. 254 (2024) 107948, https://doi.org/10.1016/j.fuproc.2023.107948.

[18] Z. Wei, H. Wang, C. Zhang, K. Xu, X. Lu, T. Lu, Reversed charge transfer and enhanced hydrogen spillover in platinum nanoclusters anchored on titanium oxide with rich oxygen vacancies boost hydrogen evolution reaction, Angew. Chem. 133 (30) (2021) 16758–16763, https://doi.org/10.1002/ange.202104856.

[19] K. Xiong, W. Yu, D.G. Vlachos, J.G. Chen, Reaction pathways of biomass-derived oxygenates over metals and carbides: from model surfaces to supported catalysts, ChemCatChem 7 (9) (2015) 1402–1421, https://doi.org/10.1002/cctc.201403067.

[20] C. Chiu, A. Genest, A. Borgna, N. Rösch, Hydrodeoxygenation of Guaiacol over Ru (0001): a DFT Study, ACS Catal. 4 (11) (2014) 4178–4188, https://doi.org/10.1021/cs500911j.

[21] Z. Luo, Z. Zheng, Y. Wang, G. Sun, H. Jiang, C. Zhao, Hydrothermally stable Ru/HZSM-5-catalyzed selective hydrogenolysis of lignin-derived substituted phenols to bio-arenes in water, Green Chem. 18 (21) (2016) 5845–5858, https://doi.org/10.1039/C6GC01971D.

[22] C. Zhao, W. Zhu, C. Liang, Role of ZrO2 crystal on the hydrodeoxygenation of methyl palmitate over NiMo/ZrO2 catalyst, Fuel 358 (2024) 130313, https://doi.org/10.1016/j.fuel.2023.130313.

[23] O. Jan, R. Marchand, L.C.A. Anjos, G.V.S. Seufitelli, E. Nikolla, F.L.P. Resende, Hydropyrolysis of lignin using Pd/HZSM-5, Energy Fuels 29 (3) (2015) 1793–1800, https://doi.org/10.1021/ef502779s.

[24] A. Saraeian, S.J. Burkhow, D. Jing, E.A. Smith, B.H. Shanks, Catalyst property effects on product distribution during the hydrodeoxygenation of lignin pyrolysis vapors over MoO_3 /γ-Al_2 O_3, ACS Sustain. Chem. Eng. 9 (19) (2021) 6685–6696, https://doi.org/10.1021/acssuschemeng.1c00295.

[25] J.P. Perdew, K. Burke, M. Ernzerhof, Generalized gradient approximation made simple, Phys. Rev. Lett. 77 (18) (1996) 3865–3868, https://doi.org/10.1103/PhysRevLett.77.3865.

[26] G. Kresse, D. Joubert, From ultrasoft pseudopotentials to the projector augmented-wave method, Phys. Rev. B 59 (3) (1999) 1758–1775, https://doi.org/10.1103/PhysRevB.59.1758.

[27] S. Grimme, J. Antony, S. Ehrlich, H. Krieg, A consistent and accurate *Ab Initio* parametrization of density functional dispersion correction (DFT-D) for the 94 elements H-Pu, J. Chem. Phys. 132 (15) (2010) 154104, https://doi.org/10.1063/1.3382344.

[28] S. Grimme, S. Ehrlich, L. Goerigk, Effect of the damping function in dispersion corrected density functional theory, J. Comput. Chem. 32 (7) (2011) 1456–1465, https://doi.org/10.1002/jcc.21759.

[29] B. Xing, J. Ma, R. Li, H. Jiao, Location, distribution and acidity of Al substitution in ZSM-5 with different Si/Al ratios – a periodic DFT computation, Catal. Sci. Technol. 7 (23) (2017) 5694–5708, https://doi.org/10.1039/C7CY01639E.

[30] Y.-K. Hong, D.-W. Lee, H.-J. Eom, K.-Y. Lee, The catalytic activity of Pd/WOx/γ-Al2O3 for hydrodeoxygenation of guaiacol, Appl. Catal. B Environ. 150–151 (2014) 438–445, https://doi.org/10.1016/j.apcatb.2013.12.045.

[31] T. Li, Y. Meng, L. Yin, B. Sun, W. Zhu, J. Su, K. Wang, Synthesis of sustainable aviation biofuels via catalytic hydropyrolysis of lignin, Appl. Catal. B Environ. Energy 353 (2024) 124092, https://doi.org/10.1016/j.apcatb.2024.124092.

[32] C. Wang, L. Guo, K. Wu, X. Li, Y. Huang, Z. Shen, H. Yang, Y. Yang, W. Wang, C. Li, Rational design of Ni-MoO3– catalyst towards efficient hydrodeoxygenation of lignin-derived bio-oil into naphthenes, J. Energy Chem. 84 (2023) 122–130, https://doi.org/10.1016/j.jechem.2023.05.029.

[33] Y. Zhang, G. Fan, L. Yang, L. Zheng, F. Li, Cooperative effects between Ni-Mo alloy sites and defective structures over hierarchical Ni-Mo bimetallic catalysts enable the enhanced hydrodeoxygenation activity, ACS Sustain. Chem. Eng. 9 (34) (2021) 11604–11615, https://doi.org/10.1021/acssuschemeng.1c04762.

[34] M. Jindal, V.C.S. Palla, B. Thallada, Effect of zeolite structure and Si/Al ratio on cotton stalks hydropyrolysis, Bioresour. Technol. 376 (2023) 128933, https://doi.org/10.1016/j.biortech.2023.128933.

[35] J. Sun, S. Shao, X. Hu, X. Li, H. Zhang, Synthesis of oxygen-containing precursors of aviation fuel via carbonylation of the aqueous bio-oil fraction followed by C–C coupling, ACS Sustain. Chem. Eng. 10 (33) (2022) 11030–11040, https://doi.org/10.1021/acssuschemeng.2c03379.

[36] V.K. Venkatakrishnan, J.C. Degenstein, A.D. Smeltz, W.N. Delgass, R. Agrawal, F. H. Ribeiro, High-pressure fast-pyrolysis, fast-hydropyrolysis and catalytic hydrodeoxygenation of cellulose: production of liquid fuel from biomass, Green Chem. 16 (2) (2014) 792, https://doi.org/10.1039/c3gc41558a.

[37] G.W. Huber, J.N. Chheda, C.J. Barrett, J.A. Dumesic, Production of liquid alkanes by aqueous-phase processing of biomass-derived carbohydrates, Science 308 (5727) (2005) 1446–1450, https://doi.org/10.1126/science.1111166.

[38] J. Jeong, H.W. Lee, S.H. Jang, S. Ryu, Y.-M. Kim, R. Park, S.-C. Jung, J.-K. Jeon, Y.-K. Park, In-situ catalytic fast pyrolysis of pinecone over HY catalysts, Catalysts 9 (12) (2019) 1034, https://doi.org/10.3390/catal9121034.

[39] D.S. Chandler, G.V.S. Seufitelli, F.L.P. Resende, Catalytic route for the production of alkanes from hydropyrolysis of biomass, Energy Fuels 34 (10) (2020) 12573–12585, https://doi.org/10.1021/acs.energyfuels.0c01548.

[40] D.C. Dayton, J. Carpenter, J. Farmer, B. Turk, R. Gupta, Biomass hydropyrolysis in a pressurized fluidized bed reactor, Energy Fuels 27 (7) (2013) 3778–3785, https://doi.org/10.1021/ef400355t.

[41] D.C. Dayton, J. Hlebak, J.R. Carpenter, K. Wang, O.D. Mante, J.E. Peters, Biomass hydropyrolysis in a fluidized bed reactor, Energy Fuels 30 (6) (2016) 4879–4887, https://doi.org/10.1021/acs.energyfuels.6b00373.

[42] L. Ren, Y. Xu, W. Chen, C. Zhang, Production of aromatic hydrocarbons from Co-hydropyrolysis of biomass components and HDPE with application of modified HZSM-5 catalyst, Chem. Biodivers. 21 (6) (2024) e202400150, https://doi.org/10.1002/cbdv.202400150.

[43] D.P. Gamliel, L. Wilcox, J.A. Valla, The effects of catalyst properties on the conversion of biomass via catalytic fast hydropyrolysis, Energy Fuels 31 (1) (2017) 679–687, https://doi.org/10.1021/acs.energyfuels.6b02781.

[44] J. Ran, L. Alfilfil, J. Li, R. Yangcheng, Z. Liu, Q. Wang, Y. Cui, T. Cao, M. Qiao, K. Yao, D. Zhang, J. Wang, Tailoring interfacial microenvironment of palladium-zeolite catalysts for the efficient low-temperature hydrodeoxygenation of vanillin in water, ChemCatChem 14 (14) (2022) e202200397, https://doi.org/10.1002/cctc.202200397.

[45] X. Liu, S. Zhang, H. Zhao, H. Lin, K. Xu, Y. Xu, L. Tan, L. Wu, Y. Tang, In-situ studies on the synergistic effect of Pd-Mo bimetallic catalyst for anisole

hydrodeoxygenation, Mol. Catal. 530 (2022) 112591, https://doi.org/10.1016/j.mcat.2022.112591.

[46] R. Gunawan, H.S. Cahyadi, R. Insyani, S.K. Kwak, J. Kim, Density functional theory investigation of the conversion of 5-(Hydroxymethyl) furfural into 2,5-dimethylfuran over the Pd(111), Cu(111), and Cu_3 Pd(111) surfaces, J. Phys. Chem. C 125 (19) (2021) 10295–10317, https://doi.org/10.1021/acs.jpcc.0c10639.

[47] B.R. Karimadom, A. Sermiagin, D. Meyerstein, T. Zidki, A. Mizrahi, R. Bar-Ziv, H. Kornweitz, Hydrogen adsorption on various transition metal (111) surfaces in water: a DFT forecast, Phys. Chem. Chem. Phys. 26 (9) (2024) 7647–7657, https://doi.org/10.1039/D3CP05884K.